MPC and SVM Design for NPC Rectifier in Hydrogen Production Application

Faghihi, T.; Bauer, P.; Vahedi, H.

DOI
10.1109/IECON58223.2025.11221936

Publication date
2025

Document Version
Final published version

Published in
Proceedings of the IECON 2025 – 51st Annual Conference of the IEEE Industrial Electronics Society

MPC and SVM Design for NPC Rectifier in Hydrogen Production Application

Tayebeh Faghihi, Pavol Bauer, Hani Vahedi
Department of Electrical Sustainable Energy, Delft University of Technology, Delft, Netherlands
Email: t.faghihisenejani@tudelft.nl, p.bauer@tudelft.nl, h.vahedi@tudelft.nl

IECON 2025 – 51st Annual Conference of the IEEE Industrial Electronics Society | 979-8-3315-9681-1/25/$31.00 ©2025 IEEE | DOI: 10.1109/IECON58223.2025.11221936

***Abstract*—This study proposes a model predictive control (MPC) strategy integrated with closed-loop space vector modulation (CL-SVM) for a three-phase, three-level neutral point clamped (3L-NPC) rectifier supplying two alkaline electrolyzers connected in series. Electrolyzers present a nonlinear and dynamically varying load due to their dependence on temperature, pressure, and electrochemical reaction rates, imposing strict requirements on the stability and responsiveness of the power supply. Among, multi-level converter topologies, the 3L-NPC rectifier is a promising candidate for low to medium-voltage, high power applications due to its reduced harmonic distortion, improved high power handling, and balanced trade-off between complexity and performance. However, maintaining DC-link capacitor voltage balance under dynamic loads remains challenging, risking power quality and system reliability. The proposed approach optimizes voltage vector selection to regulate DC output and minimize neutral-point voltage deviation. Simulation results in MATLAB/Simulink confirm the effectiveness of the designed controller in achieving stable DC voltage and a balanced neutral-point voltage, thereby enhancing the overall performance of the power-electronics interface in electrolyzer applications.**

***Index Terms*—Hydrogen Production, Model Predictive Control (MPC), Neutral Point Clamped (NPC) Rectifier, Space Vector Modulation (SVM), Voltage Balancing.**

I. Introduction

The transition toward carbon-neutral energy systems has accelerated the development of green hydrogen as a sustainable energy carrier, with water electrolysis powered by renewable electricity emerging as an important technology supporting the mass production of hydrogen [1]. Electrolyzers require a stable and well-regulated direct current (DC) supply, making power electronic rectifiers a critical interface between the electrical grid and the electrochemical process [2]. A rectifier is a fundamental power electronic converter designed to transform an alternating current (AC) into DC, typically classified into uncontrolled and controlled categories. Uncontrolled rectifiers use passive devices such as diodes, while controlled rectifiers employ actively switched devices such as thyristors, MOSFETs, or IGBTs to enable dynamic regulation of the output [3].

In advanced applications requiring improved power quality and reduced electromagnetic interference, multilevel converter topologies have emerged as a promising solution. These converters offer advantages such as reduced total harmonic distortion (THD), lower switching losses, and operation at higher power levels without increasing the stress on individual semiconductor devices [4]–[8]. Among various multilevel structures, the neutral point clamped (NPC) converter is widely adopted due to its balanced trade-off between circuit complexity, efficient voltage sharing through clamping diodes, and reduced device voltage stress [9]. Despite its advantages, the NPC topology faces a key challenge in maintaining DC-link capacitor voltage balance, especially under dynamic loading [10]. Under ideal operating conditions, the midpoint potential should remain stable to ensure equal voltage sharing and minimize circulating currents.

However, due to unequal switching states, asymmetric current flow, or imbalanced load power, the neutral-point potential may drift, resulting in unequal capacitor voltages. This imbalance can increase voltage stress on semiconductor devices, degrade power quality, and compromise long-term system reliability [11]. To mitigate this issue, several voltage balancing strategies have been proposed in the literature, including modified PWM techniques [12]–[15], hybrid neutral-point voltage controllers [16], [17], and the use of redundant switching states and space vector modulation (SVM) [18]–[20]. Effective implementation of these control methods is crucial for stable operation, particularly in applications such as electrolyzers, where the load exhibits nonlinear and time-varying characteristics. However, most of these methods have been developed and validated primarily for inverter operation, where the power flows from the DC-link to the AC side. In contrast, the rectifier mode of operation, especially under unbalanced or time-varying load conditions, such as those encountered in electrolyzer systems, has received comparatively less attention and requires further investigation to develop robust and effective voltage balancing strategies.

Although several control strategies, such as proportional-integral (PI) regulators, redundant switching state selection, and modified modulation techniques, have been proposed to address the neutral-point voltage balancing issue in NPC converters, many of these approaches are based on static control logic or heuristic design, which limits their performance under dynamic operating conditions. Moreover, these methods typically lack predictive capabilities and are unable to simultaneously address multiple control objectives, such as maintaining DC-link voltage regulation and neutral-point voltage stability. To overcome these limitations, this paper proposes a hybrid control strategy that integrates Model Predictive Control (MPC) with closed-loop space vector modulation (CL-SVM) for a 3L-NPC rectifier that supplies two alkaline electrolyzers connected in series and operating under the same conditions. In contrast to conventional finite-set MPC

methods that directly select switching states, the proposed approach predicts the optimal three-phase rectifier voltage vector to regulate the DC output voltage and minimize the neutral-point voltage deviation. This voltage reference is then applied using a CL-SVM scheme enabling high-quality current waveforms and efficient switching operation. By combining MPC's capabilities with SVM's implementation advantages, the proposed hybrid method achieves improved DC voltage regulation, effective neutral-point balancing, and enhanced system stability.

The remainder of the paper is organized as follows. Section II provides an overview of the system. Section III details the system modeling and the proposed control strategy. Section IV presents the simulation results, demonstrating the effectiveness of the proposed method. Section V concludes the paper and outlines potential directions for future research.

II. System Overview

A. Three-level neutral point clamped rectifier

The NPC converter, also known as the diode-clamped multilevel converter, is one of the most widely adopted multilevel topologies for various applications. As illustrated in Fig. 1, it consists of four switches and two clamping diodes per leg, connected to the midpoint of the DC-link capacitors [21]. Table I presents the switching states and associated phase-leg voltages with respect to the DC-link midpoint for a single leg of the NPC rectifier topology.

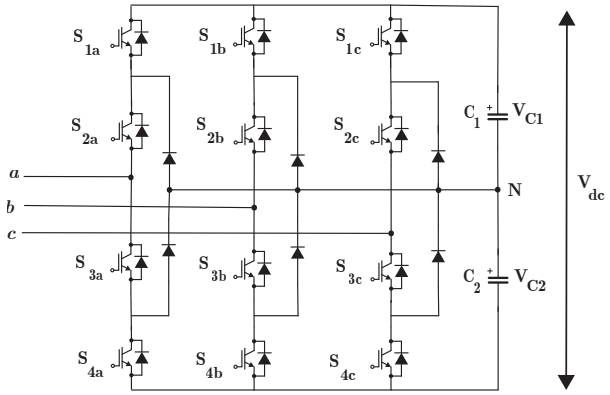

Fig. 1. Three-level three-phase neutral point clamped (NPC) rectifier

TABLE I
Switching States of Three-Level NPC Rectifier

S_{1a}	S_{2a}	S_{3a}	S_{4a}	Phase Leg Voltage
1	1	0	0	$+V_{dc}/2$
0	1	1	0	0
0	0	1	1	$-V_{dc}/2$

This configuration achieves multiple voltage levels through the use of clamping diodes and split DC-link capacitors, enabling the output voltage to alternate between positive, neutral, and negative levels. It is important to note that the switches S_{3a} and S_{4a} operate as complementary counterparts of S_{1a} and S_{2a}, respectively. Consequently, only two independent gate signals are required to control all four switches.

B. Principle of Water Electrolysis

Fig. 2 illustrates the fundamental operating mechanism of water electrolysis, where water is decomposed into hydrogen and oxygen through electrochemical reactions facilitated by an external DC power supply [22]. Water electrolysis technologies include Alkaline, Proton Exchange Membrane (PEM), Anion Exchange Membrane (AEM), and Solid Oxide Electrolyzers (SOE) [23]. In this work, the alkaline electrolyzer is adopted because of its technological maturity, lower cost, and suitability for steady-state operation.

The system consists of two electrodes, a cathode and an anode, submerged in an aqueous alkaline electrolyte, commonly potassium hydroxide (KOH). A permeable separator is placed between the electrodes to facilitate the selective movement of hydroxide ions (OH^-) from the cathode to the anode, while inhibiting the mixing of the produced gases. The cathode triggers the reduction of water molecules to produce hydrogen gas and hydroxide ions, while the anode drives the oxidation of hydroxide ions, generating oxygen gas and water. This electrochemical process is characterized by relatively low operating temperatures (typically 60–90 °C) and is widely used due to its mature technology and stable long-term performance [24].

Equation (1) describes the overall water electrolysis reaction, with equations (2) and (3) detailing the half-reactions occurring at the cathode and anode, respectively [25]:

$$\mathrm{H_2O\ (l)} \rightarrow \mathrm{H_2\ (g)} + \tfrac{1}{2}\mathrm{O_2\ (g)} \tag{1}$$

$$2\mathrm{H_2O\ (l)} + 2e^- \rightarrow \mathrm{H_2\ (g)} + 2\mathrm{OH^-\ (aq)} \tag{2}$$

$$2\mathrm{OH^-\ (aq)} \rightarrow \mathrm{H_2O\ (l)} + \tfrac{1}{2}\mathrm{O_2\ (g)} + 2e^- \tag{3}$$

C. Electrolyzer Modeling Approach

For alkaline electrolyzers, electrical modeling can be categorized into two main types: static and dynamic. The static model, also referred to as the resistive model, comprises a voltage source representing the reversible voltage, the minimum voltage required to initiate electrolysis, and a series resistance accounting for ohmic losses. Although this model provides a simplified representation suitable for steady-state analysis, it does not capture transient phenomena observed during dynamic operation.

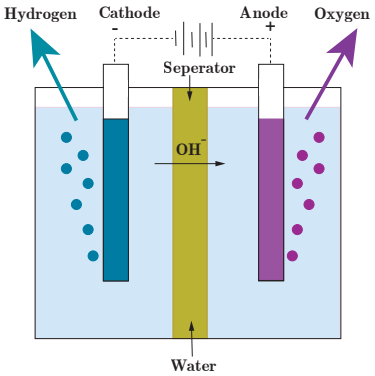

Fig. 2. Principle of electrolysis of water [26]

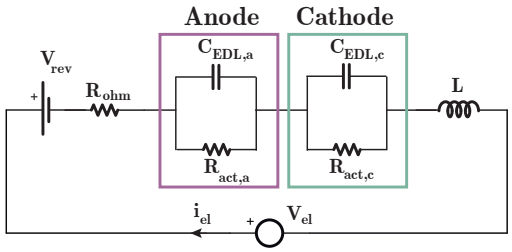

Fig. 3. Dynamic equivalent circuit for Alkaline electrolyzer [27]

To enhance the accuracy of this representation, a dynamic model can be employed, as illustrated in Fig. 3. This model incorporates the effect of the electric double layer (EDL), which refers to the formation of a potential difference at the electrode–electrolyte interface, even in the absence of current flow. This phenomenon is typically modeled using a capacitor. In addition, an inductance is introduced to account for the inertial delay in the current response, particularly during rapid changes in load or control signals. Activation resistances are also included at the anode and cathode to represent the energy barriers associated with electrochemical reactions.

By incorporating these dynamic elements, the model offers a more accurate representation of the electrolyzer's electrical dynamics during transient operating conditions. The remaining components of the circuit are consistent with those in the static model [27].

III. System Modelling and Control

The system considered in this study is shown in Fig. 4. On the AC side, $v_{g,a}$, $v_{g,b}$, and $v_{g,c}$ represent the three-phase grid voltages, and i_{abc} denotes the three-phase filter current. The filter is composed of an inductance L_g and an equivalent series resistance R_g.

On the DC side, the total DC-link voltage is denoted by V_{dc}, and the voltages across capacitors C_1 and C_2 are denoted by V_{C1} and V_{C2}, respectively.

As described in the following sections, the proposed control scheme consists of multiple interconnected modules, including:

- Grid synchronization and *dq* transformation
- Outer-loop DC voltage control
- Inner-loop model predictive current control
- Neutral-point voltage balancing
- Switching state selection and modulation using CL-SVM

A. dq Model of the MPC Current Control

Grid synchronization is essential for the stable operation of a grid-connected rectifier. This is accomplished by implementing a phase-locked loop (PLL) algorithm that continuously monitors the phase angle of the grid voltage. This angle is then provided to the current control loop, ensuring accurate alignment between the converter's operation and the grid—critical for achieving sinusoidal input currents and maintaining power quality.

The proposed strategy employs model predictive current control for a three-level, three-phase NPC rectifier using *dq*-frame transformation. It takes the grid voltage $v_{g,abc}$, phase currents i_{abc}, DC-link voltage V_{dc}, capacitor voltages V_{C1} and V_{C2}, grid angle θ, and reference DC voltage $V_{dc,ref}$ as inputs.

First, v_{abc} and i_{abc} are transformed into the *dq* reference frame using the Park transformation:

$$T_{dq0} = \frac{2}{3}\begin{bmatrix} \cos(\theta) & \cos(\theta-\frac{2\pi}{3}) & \cos(\theta+\frac{2\pi}{3}) \\ -\sin(\theta) & -\sin(\theta-\frac{2\pi}{3}) & -\sin(\theta+\frac{2\pi}{3}) \\ \frac{1}{2} & \frac{1}{2} & \frac{1}{2} \end{bmatrix} \quad (4)$$

The system dynamics in the synchronous frame is described by the RL filter model:

$$\frac{di_d}{dt} = \frac{1}{L}\left(v_{rect,d} - Ri_d - v_{g,d} + \omega L i_q\right) \quad (5)$$

$$\frac{di_q}{dt} = \frac{1}{L}\left(v_{rect,q} - Ri_q - v_{g,q} - \omega L i_d\right) \quad (6)$$

These equations are discretized using Euler approximation:

$$i_d[k{+}1] = i_d[k] + \frac{T_s}{L}\left(v_{rect,d}[k] - Ri_d[k] - v_{g,d}[k] + \omega L i_q[k]\right) \quad (7)$$

$$i_q[k{+}1] = i_q[k] + \frac{T_s}{L}\left(v_{rect,q}[k] - Ri_q[k] - v_{g,q}[k] - \omega L i_d[k]\right) \quad (8)$$

A PI controller is used in the outer loop to regulate the DC-link voltage, producing the current reference of the d axis:

$$i_{d,ref} = K_p(V_{dc,ref} - V_{dc}) + K_i \int (V_{dc,ref} - V_{dc})\, dt \quad (9)$$

Where K_p and K_i are the proportional and integral gains, respectively. Assuming unity power factor, the q-axis current reference is set to:

$$i_{q,ref} = 0 \quad (10)$$

The control law then calculates the required *dq* voltages based on the discrete-time model of the L-filtered converter:

$$v_{rect,d} = v_{g,d} - Ri_d + \omega L i_q - \frac{L}{T_s}(i_{d,ref} - i_d) \quad (11)$$

$$v_{rect,q} = v_{g,q} - Ri_q + \omega L i_d - \frac{L}{T_s}(i_{q,ref} - i_q) \quad (12)$$

To ensure that the capacitor voltage remains balanced across the DC-link midpoint, a feedback correction term is added to $v_{rect,d}$:

$$\Delta v_{rect,d} = K_{np}(V_{C1} - V_{C2}) \cdot \text{sign}(i_d) \quad (13)$$

Where K_{np} is the neutral-point balancing gain. This term is bounded to a practical range to avoid instability or excessive correction.

Finally, the computed rectifier voltage references $v_{rect,d}$ and $v_{rect,q}$ are transformed back to the three-phase *abc* frame using the inverse Park transformation:

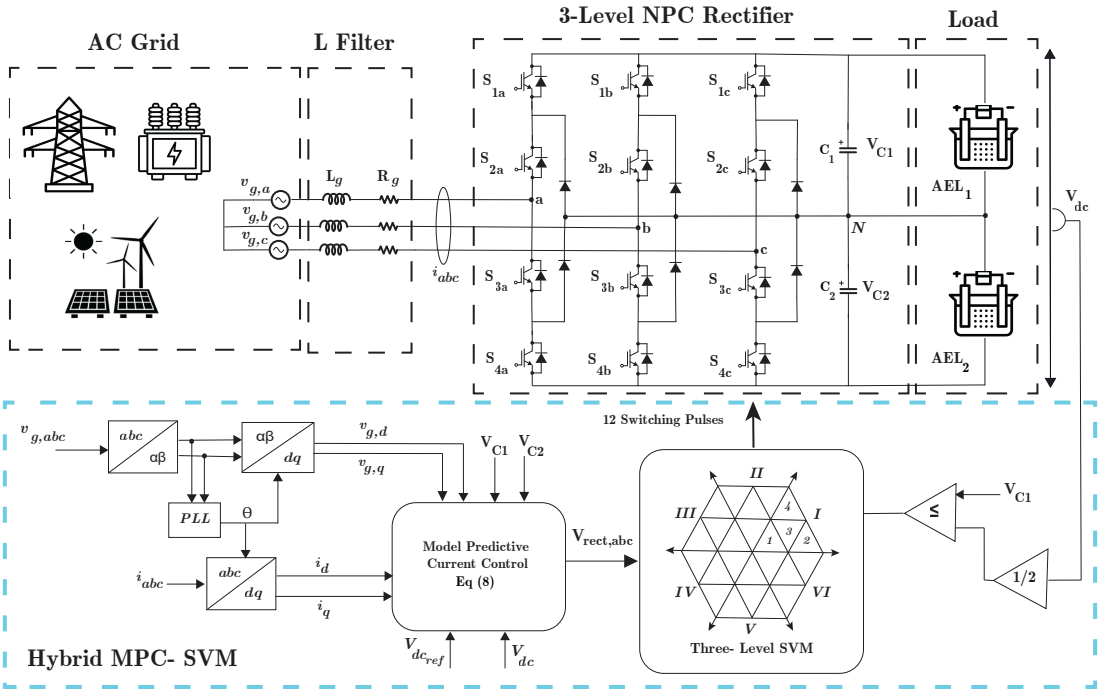

Fig. 4. Overall MPC- SVM design applied to Three- Level NPC rectifier.

$$T_{dq}^{-1} = \begin{bmatrix} \cos(\theta) & -\sin(\theta) \\ \cos(\theta - \frac{2\pi}{3}) & -\sin(\theta - \frac{2\pi}{3}) \\ \cos(\theta + \frac{2\pi}{3}) & -\sin(\theta + \frac{2\pi}{3}) \end{bmatrix} \tag{14}$$

The resulting vector $v_{rect,abc}$ provides the reference voltages to be used in a three-level SVM scheme to determine the appropriate switching states of the NPC rectifier.

B. Space Vector Modulation (SVM)

Space Vector Modulation is a widely adopted pulse-width modulation technique for NPC converters due to its efficient utilization of the DC-link voltage, lowered total harmonic distortion, and flexible switching state selection [28]. Compared to conventional two-level converters, the three-level SVM expands the space vector diagram into additional sectors and regions, introducing a greater number of voltage vectors, including redundant switching states that can generate the same output vector.

These redundancies provide an opportunity to implement advanced control objectives such as neutral-point voltage balancing. To achieve this, the switching state selection process incorporates a correction mechanism based on the voltage imbalance between the two DC-link capacitors.

In the proposed method, referred to as closed-loop SVM (CL-SVM), the voltage of the upper capacitor V_{C1} is compared to half of the DC-link voltage $V_{dc}/2$. When a deviation is detected (i.e., $V_{C1} \neq V_{dc}/2$), the SVM algorithm dynamically prioritizes those redundant switching states that contribute to restoring the neutral-point voltage balance.

This strategy ensures that switching states account not only for accurate tracking of the reference voltage vector but also for the sign and magnitude of the neutral-point deviation. By embedding this feedback mechanism into the modulation stage, the control system effectively mitigates long-term voltage drift at the DC midpoint, thereby ensuring balanced capacitor voltages and improving the overall stability and reliability of the NPC rectifier.

IV. Simulation Results and Discussion

To verify the performance of the proposed control strategy, a three-phase NPC rectifier connected to the grid and supplying 25 kW electrolyzers as load is simulated using MATLAB/Simulink. In the configuration, each DC-link capacitor is connected to a separate electrolyzer, both operating under identical conditions.

The detailed system parameters applied in the simulation are listed in Table II. A sampling time of $T_s = 20\,\mu s$ is adopted throughout the simulation to ensure accurate dynamic response and high resolution control performance.

TABLE II
Parameters of the Simulated System

Parameter	Value
Grid voltage	230 V (peak)
Grid frequency	50 Hz
Line inductors	2.5 mH, each
Line resistors	0.1 Ω, each
DC bus capacitors	2700 μF, each
Switching frequency	5 kHz
Ohmic resistance, R_{ohmic}	0.5 Ω
Filter inductance, L	0.025H
Activation resistance (Anode), $R_{act,a}$	0.33 Ω
Activation resistance (Cathode), $R_{act,c}$	0.16 Ω
Electric double layer capacitance, C_{EDL}	0.1081F
Reversible voltage, V_{rev}	200 V

Figures 5 to 10 illustrate the simulation results of the proposed MPC-SVM algorithm under both normal operating conditions and external disturbances applied to the DC side.

Fig. 5 presents the DC output voltage (V_{dc}) and current (i_{dc}), along with the voltages of the individual DC-link capacitors. All waveforms exhibit minimal ripple under steady-state conditions, demonstrating effective voltage regulation, accurate load tracking, and well-balanced capacitor voltages.

The rectifier input voltage waveform in Fig. 6 confirms a well-defined five-level symmetrical output. This highlights the modulator's capability to synthesize high-quality voltage levels, enhancing both voltage balancing and harmonic performance.

Fig. 7 shows the grid voltage (v_a) and three-phase currents (i_{abc}), where the voltage and current of phase "a" are observed to be in phase. Fig. 8 shows a near-unity power factor, exceeding 99.9% after the transient period, indicating efficient power conversion with minimal reactive power flow. The total harmonic distortion (THD) of the grid current, as shown in Fig. 9, is 2.75%, remaining within the acceptable limits defined by international standards such as IEEE 519-2022.

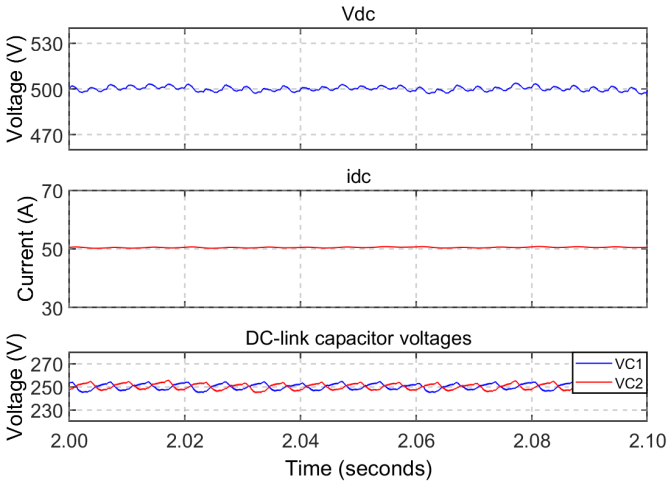

Fig. 5. Total load-side DC voltage (top), DC current (middle), and voltages of the upper and lower DC-link capacitors (bottom)

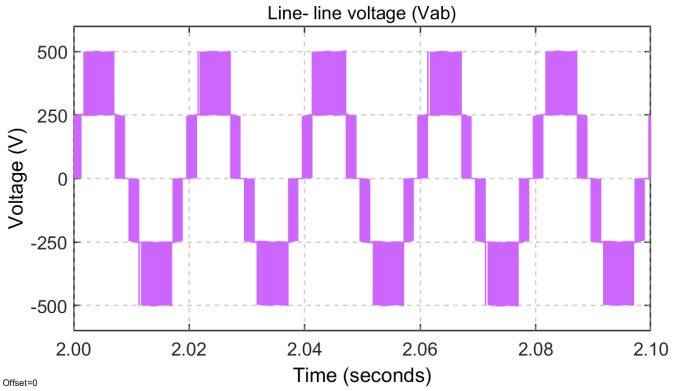

Fig. 6. Five- level line-line voltage (V_{ab}) in the rectifier input

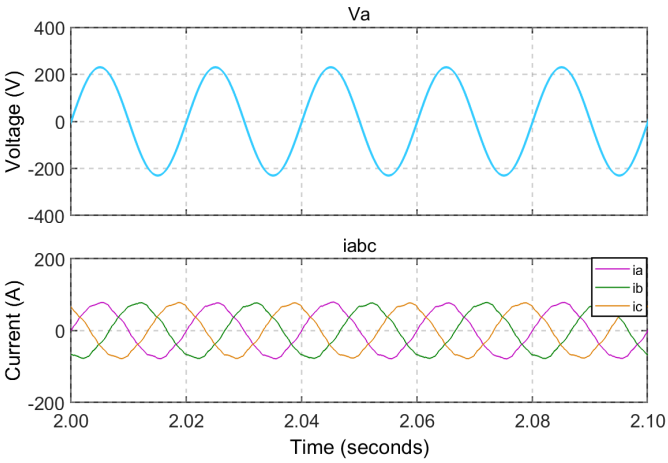

Fig. 7. Grid-side phase "a" voltage (top) and three-phase current (bottom)

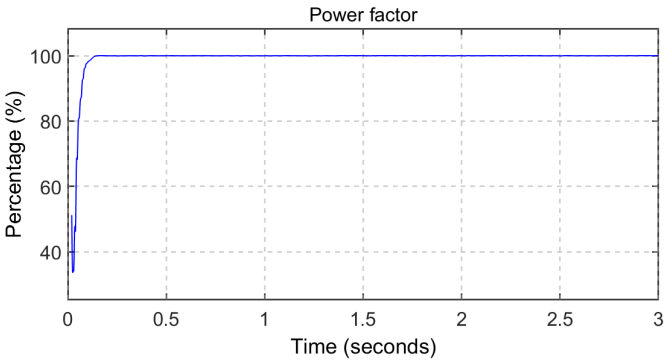

Fig. 8. Power factor on the AC side

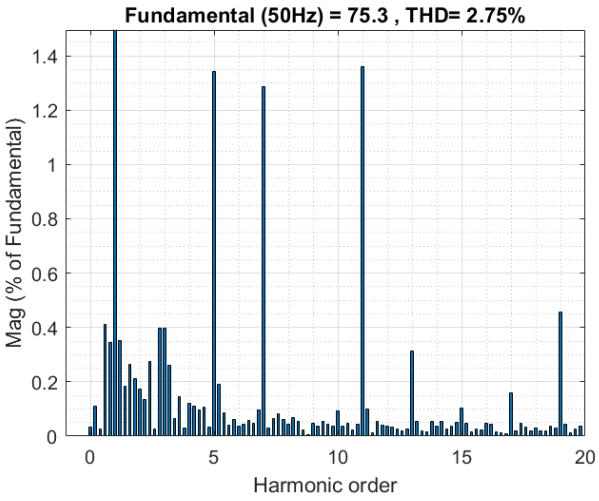

Fig. 9. Total Harmonic Distortion of grid-side current phase "a"

Fig. 10 shows the system response to a disturbance on the DC side. In this scenario, the system remains stable, underscoring the robustness and strong disturbance rejection capability of the proposed MPC-SVM strategy.

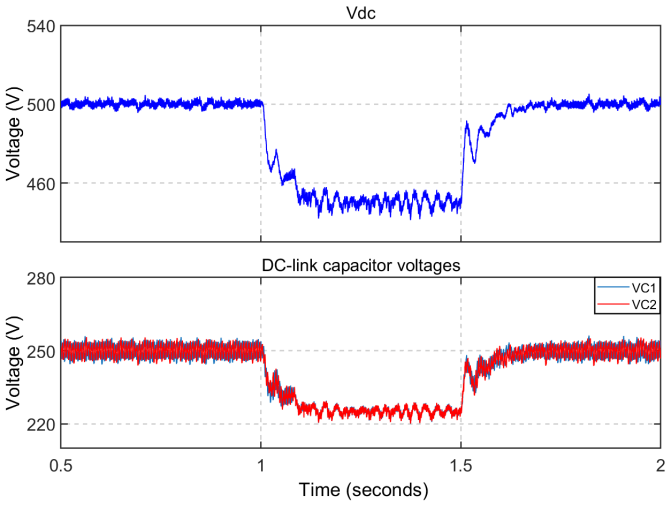

Fig. 10. Results during a reference DC voltage variation (from 500V to 450V and back)

V. Conclusion

This paper presented a hybrid MPC strategy combined with CL-SVM for a three-phase, 3L-NPC rectifier that supplies alkaline electrolyzers. The proposed approach effectively mitigates the neutral-point voltage imbalance by predicting optimal voltage vectors to regulate the DC-link voltage while maintaining the capacitor voltage balance. The simulation results demonstrate stable operation at a switching frequency of 5kHz, improved power quality (THD $< 2.75\%$ and power factor $> 99.9\%$), and enhanced reliability under dynamic electrolyzer load conditions. Future work will explore the extension of this control framework to electrolyzers operating under varying and uncertain conditions and the integration of detailed electrolyzer models to support the development of adaptive strategies for optimal green hydrogen production.

References

[1] M. Jayachandran, R. K. Gatla, A. Flah, A. H. Milyani, H. M. Milyani, V. Blazek, L. Prokop, and H. Kraiem, "Challenges and opportunities in green hydrogen adoption for decarbonizing hard-to-abate industries: A comprehensive review," *IEEE Access*, vol. 12, pp. 23 363–23 388, 2024.

[2] R. S. Deshmukh, G. Rituraj, P. Bauer, and H. Vahedi, "Real-time digital twin implementation of power electronics-based hydrogen production system," *Energy Reports*, vol. 13, pp. 5006–5015, 2025.

[3] M. H. Rashid, Ed., *Power Electronics Handbook*, 4th ed. Amsterdam: Elsevier Butterworth–Heinemann, 2017.

[4] H. Vahedi, "5-level packed u-cell (puc5) active front-end rectifier," *IEEE Open Journal of Power Electronics*, vol. 6, pp. 1022–1027, 2025.

[5] H. Vahedi and M. Trabelsi, *Single-DC-Source Multilevel Inverters*, 1st ed., ser. SpringerBriefs in Electrical and Computer Engineering. Springer Cham, 2019.

[6] H. V. Al-Haddad, "Method and system for operating a multilevel electric power inverter," Patent US9 923 484B2, 2018, assigned U.S. Patent.

[7] H. Vahedi, P.-A. Labbé, and K. Al-Haddad, "Sensor-less five-level packed u-cell (puc5) inverter operating in stand-alone and grid-connected modes," *IEEE Transactions on Industrial Informatics*, vol. 12, no. 1, pp. 361–370, 2016.

[8] M. Trabelsi, H. Vahedi, and H. Abu-Rub, "Review on single-dc-source multilevel inverters: Topologies, challenges, industrial applications, and recommendations," *IEEE Open Journal of the Industrial Electronics Society*, vol. 2, pp. 112–127, 2021.

[9] J. Rodriguez, S. Bernet, P. K. Steimer, and I. E. Lizama, "A survey on neutral-point-clamped inverters," *IEEE Transactions on Industrial Electronics*, vol. 57, no. 7, pp. 2219–2230, 2010.

[10] S. Busquets Monge, S. Somavilla, J. Bordonau, and D. Boroyevich, "Capacitor voltage balance for the neutral-point- clamped converter using the virtual space vector concept with optimized spectral performance," *IEEE Transactions on Power Electronics*, vol. 22, no. 4, pp. 1128–1135, 2007.

[11] M. Trabelsi, A. N. Alquennah, and H. Vahedi, "Review on single-dc-source multilevel inverters: Voltage balancing and control techniques," *IEEE Open Journal of the Industrial Electronics Society*, vol. 3, pp. 711–732, 2022.

[12] P. Zhang, X. Wu, B. Li, L. Ding, J. Long, W. Zhang, and Y. Li, "A zero-sequence component injection pwm scheme for three-level neutral point clamped rectifiers with unbalanced dc-link voltages," *IEEE Transactions on Industrial Electronics*, vol. 71, no. 6, pp. 5420–5430, 2024.

[13] S. K. Giri, S. Chakrabarti, S. Banerjee, and C. Chakraborty, "A carrier-based pwm scheme for neutral point voltage balancing in three-level inverter extending to full power factor range," *IEEE Transactions on Industrial Electronics*, vol. 64, no. 3, pp. 1873–1883, 2017.

[14] L. Ben-Brahim, "A discontinuous pwm method for balancing the neutral point voltage in three-level inverter-fed variable frequency drives," *IEEE Transactions on Energy Conversion*, vol. 23, no. 4, pp. 1057–1063, 2008.

[15] K. Chen, W. Jiang, and P. Wang, "An extended dpwm strategy with unconditional balanced neutral point voltage for neutral point clamped three-level converter," *IEEE Transactions on Industrial Electronics*, vol. 66, no. 11, pp. 8402–8413, 2019.

[16] W. Wan, S. Duan, C. Chen, and T. Yu, "A hybrid control method for neutral-point voltage balancing in three-level inverters," *IEEE Transactions on Power Electronics*, vol. 36, no. 8, pp. 8575–8582, 2021.

[17] F. Sebaaly, H. Vahedi, H. Y. Kanaan, N. Moubayed, and K. Al-Haddad, "Model predictive controller with fixed switching frequency for a 3l-npc inverter," in *IECON 2016 - 42nd Annual Conference of the IEEE Industrial Electronics Society*, 2016, pp. 6536–6511.

[18] V. Jayakumar, B. Chokkalingam, and J. L. Munda, "A comprehensive review on space vector modulation techniques for neutral point clamped multi-level inverters," *IEEE Access*, vol. 9, pp. 112 104–112 144, 2021.

[19] A. Zorig, S. Barkat, and A. Sangwongwanich, "Neutral point voltage balancing control based on adjusting application times of redundant vectors for three-level npc inverter," *IEEE Journal of Emerging and Selected Topics in Power Electronics*, vol. 10, no. 5, pp. 5604–5613, 2022.

[20] P. Qashqai, A. Sheikholeslami, H. Vahedi, and K. Al-Haddad, "A new svm-based voltage balancing method for five-level npc inverter," in *2016 7th Power Electronics and Drive Systems Technologies Conference (PEDSTC)*, 2016, pp. 511–516.

[21] A. Nabae, I. Takahashi, and H. Akagi, "A new neutral-point-clamped pwm inverter," *IEEE Transactions on Industry Applications*, vol. IA-17, no. 5, pp. 518–523, 1981.

[22] A. Ursua, L. M. Gandia, and P. Sanchis, "Hydrogen production from water electrolysis: Current status and future trends," *Proceedings of the IEEE*, vol. 100, no. 2, pp. 410–426, 2012.

[23] A. Buttler and H. Spliethoff, "Current status of water electrolysis for energy storage, grid balancing and sector coupling via power-to-gas and power-to-liquids: A review," *Renewable and Sustainable Energy Reviews*, vol. 82, pp. 2440–2454, 2018.

[24] K. Zeng and D. Zhang, "Recent progress in alkaline water electrolysis for hydrogen production and applications," *Progress in Energy and Combustion Science*, vol. 36, no. 3, pp. 307–326, 2010.

[25] A. Iribarren, E. Barrios, H. Ibaiondo, A. Sanchez-Ruiz, J. Arza, P. Sanchis, and A. Ursúa, "Dynamic modeling and simulation of a pressurized alkaline water electrolyzer: a multiphysics approach," in *2021 IEEE International Conference on Environment and Electrical Engineering and 2021 IEEE Industrial and Commercial Power Systems Europe (EEEIC / ICPS Europe)*, 2021, pp. 1–6.

[26] E. O. Ogundimu and C. Graham Richards, "Enhancing green hydrogen production and sustainability," in *2025 33rd Southern African Universities Power Engineering Conference (SAUPEC)*, 2025, pp. 1–6.

[27] J. V. Ferrando, "Modelling and simulation of hydrogen electrolyzers for power system applications," Master of science thesis, [KTH Royal Institute of Technology], 2023.

[28] P. Qashqai, H. Vahedi, A. Sheikholeslami, and K. Al-Haddad, "A general space-vector modulation technique for multilevel npc inverter," in *2016 IEEE International Conference on Industrial Technology (ICIT)*, 2016, pp. 1202–1207.